Published in final edited form as:
Neuroscience. 2014 January 17; 257: 96–110. doi:10.1016/j.neuroscience.2013.10.065.

Heterogeneous intrinsic excitability of murine spiral ganglion neurons is determined by K_v1 and HCN channels

Qing Liu[a], **Edmund Lee**[b], and **Robin L. Davis**[a]

[a]Department of Cell Biology and Neuroscience, Rutgers University, Piscataway, NJ 08854, USA

[b]Rutgers University - New Jersey Medical School, Newark, NJ 07746, USA

Abstract

The spiral ganglion conveys afferent auditory information predominantly through a single class of type I neurons that receive signals from inner hair cell (IHC) sensory receptors. These auditory primary afferents, like in other systems (Puopolo and Belluzzi, 1998, Gascon and Moqrich, 2010, Leao et al., 2012) possess a marked diversity in their electrophysiological features (Taberner and Liberman, 2005). Consistent with these observations, when the auditory primary afferents were assessed in neuronal explants separated from their peripheral and central targets it was found that individual neurons were markedly heterogeneous in their endogenous electrophysiological features. One aspect of this heterogeneity, obvious throughout the ganglion, was their wide range of excitability as assessed by voltage threshold measurements (Liu and Davis, 2007). Thus, while neurons in the base differed significantly from apical and middle neurons in their voltage thresholds, each region showed distinctly wide ranges of values. To determine whether the resting membrane potentials (RMP) of these neurons correlate with the threshold distribution and to identify the ion channel regulatory elements underlying heterogeneous neuronal excitability in the ganglion, patch-clamp recordings were made from postnatal day (P5-8) murine spiral ganglion neurons in vitro. We found that RMP mirrored the tonotopic threshold distribution, and contributed an additional level of heterogeneity in each cochlear location. Pharmacological experiments further indicated that threshold and RMP was coupled through the K_v1 current, which had a dual impact on both electrophysiological parameters. Whereas, hyperpolarization-activated cationic channels (HCN) decoupled these two processes by primarily affecting RMP without altering threshold level. Thus, beyond mechanical and synaptic specializations, ion channel regulation of intrinsic membrane properties imbues spiral ganglion neurons with different excitability levels, a feature that contributes to primary auditory afferent diversity.

Keywords

spiral ganglion neuron; intrinsic excitability; K_v1; I_h; auditory

The spiral ganglion is a model system well-suited for studying the complex endogenous properties of a predominantly single class of neurons with defined synaptic input and

Corresponding author: Dr. Robin L. Davis, Department of Cell Biology & Neuroscience, 604 Allison Road, Nelson Laboratories, Rutgers University, Piscataway, NJ 08854, rldavis@rci.rutgers.edu. Phone: 732-445-0440, FAX: 732-445-5870.

Disclosures: No conflicts of interest, financial or otherwise, are declared by the authors.

function (Raphael and Altschuler, 2003). In addition to the wide variety of features that tailor the auditory sensory receptors along the frequency axis of the cochlea in mammals, birds, and reptiles (Corwin and Warchol, 1991), the endogenous features of mammalian postnatal spiral ganglion neurons can also be distinguished tonotopically (Davis and Liu, 2011). Their morphological profile is stereotypically mapped according to frequency of innervation (Liberman and Oliver, 1984, Nadol et al., 1990, Ryugo, 1992, Rosbe et al., 1996, Echteler and Nofsinger, 2000) and the electrophysiological profile of postnatal neurons also varies systematically. Previous studies showed that even when spiral ganglion neurons were separated from their peripheral and central targets, their endogenous firing features were not identical (Mo and Davis, 1997, Adamson et al., 2002b, Reid et al, 2004). Timing characteristics measured at threshold, such as onset time course, action potential latency and duration, varied linearly according to their basal to apical cochlear innervation, and thus were potentially associated with frequency coding (Liu and Davis, 2007). On the other hand, for this same data set, voltage thresholds for firing were lowest in the middle and apical cochlear regions but highest in the base despite their distinctly heterogeneous levels within each frequency region.

This is an intriguing result because it suggests that the very same group of neurons that display linearly graded timing features simultaneously possess heterogeneous, nonlinear threshold levels. In order to understand better the elements that orchestrate this complex intrinsic organization, we sought to identify the underlying ion channels that control two features related to intrinsic excitability, voltage threshold and resting membrane potential (RMP), to complement our previous characterization of ionic regulation of firing timing (Adamson et al., 2002b). Furthermore, we explore how the heterogeneity of neuronal excitability is achieved within the spiral ganglion.

The results reported herein identify two channel types, K_v1 and HCN, which play a role in determining the excitability of spiral ganglion neurons. Pharmacological experiments with α-dendrotoxin (DTX) to block K_v1 not only altered accommodation in spiral ganglion neurons (Mo et al., 2002), but, as shown herein, also affected voltage threshold and RMP. This later observation was substantiated with whole-cell voltage clamp experiments and showed that DTX-subtracted current amplitudes were significantly higher in the basal, high threshold neurons than in the apical, low threshold neurons. Consistent with this finding, the least sensitive base neurons were the most intensely labeled with both anti-$K_v1.1$ and anti-$K_v1.2$ antibodies compared to middle and apical neurons. We also found that HCN channels contributed to setting the RMP without affecting threshold level, indicating that resting potential regulation can be decoupled from threshold regulation. Thus, our results suggest that differential combinations of HCN and K_v1 channel densities define the distribution and correlation of neuronal resting potential and threshold levels that together contributes to enhancing spiral ganglion heterogeneity.

Experimental procedures

Tissue culture

Cochleae were removed from postnatal day 5 to 8 (P5–P8) CBA/CaJ mice; ages with good viability *in vitro*, allowing maximal numbers of high quality recordings. The spiral ligament, stria vascularis, and organ of Corti were removed to isolate the spiral ganglion. Location-dependent features were studied using *neuronal cultures*, in which the ganglion was uncoiled and then divided into fifths using fine forceps; three of these five regions (base, middle, and apex but not base-middle or middle-apex) were plated into separate culture dishes. All spiral ganglion tissues were plated on poly-L-lysine-coated dishes and maintained in growth medium (Dulbecco's modified Eagle's medium [DMEM], supplemented with 10% fetal bovine serum, 4 mM L-glutamine, and 0.1% penicillin-streptomycin) for 5–22 days *in*

vitro (DIV) at 37°C in a humidified incubator with 5% CO_2. The differential tonotopic distribution of neuronal electrophysiological properties was not detectably affected by DIV used in this and a previous study (Adamson et al., 2002b); therefore the data were grouped. Sun and Salvi (Sun and Salvi, 2009) detected an effect of DIV on spiral ganglion neuron firing but this effect was largely restricted to the first 3 DIV and may be due to the use of trypsin to facilitate dissociation of neurons; a treatment that can influence neuronal properties (Kim et al., 2012). This concern would not affect our studies as our explanted cultures are not subjected to enzymatic treatment. Procedures performed on CBA/CaJ mice were approved by the Rutgers University Institutional Review Board for the Use and Care of Animals (IRB-UCA), protocol 90-073.

Immunofluorescence

Tissue was fixed in 100% methanol (−20°C for 6 min) and rinsed three times with 0.01 M phosphate-buffered saline (PBS; pH 7.4) for 5 min. Prior to each primary antibody application, tissue was incubated with 5% normal goat serum (NGS) for 1 h to block non-specific labeling. The primary antibody was applied and the tissue was incubated for 1 h at room temperature or overnight at 4°C, then rinsed three times with PBS for 5 min. Fluorescein-conjugated secondary antibody (anti-mouse Alex-Flour 594/488, 1:100, Invitrogen, 11020/11017 or anti-rabbit Alex-Flour 488, 1:100, Invitrogen, 11070) was subsequently applied for 1 h at room temperature. Controls to assess immunostaining with secondary antibody alone, in which the primary antibody was replaced with blocking solution, showed no appreciable labeling. The preparations were then rinsed three times with PBS for 5 min. DABCO (1, 4-diazabicyclo [2.2.2] octane) was applied at the end to the preparation for viewing and storage. Images were acquired with a Hamamatsu ORCA-ER camera on a Zeiss Axiovert 200M inverted microscope controlled by IPLab software (Scanalytics, Inc.). The same exposure time was used to acquire images within each experiment. The antibody luminance was measured in IPLab with no digital enhancement by subtracting the mean of 144 pixels at four background areas from the mean of 108 pixels at three brightest areas inside each neuron.

The primary antibodies used are as follows: monoclonal anti-β-tubulin (1:350, Covance, MMS-435P, β-TUJ1), polyclonal anti-β-tubulin (1:200, Covance, PRB-435P), monoclonal anti-K_v1.1 (1:40, UC Davis/NIH NeuroMab Facility, K36/15), monoclonal anti-K_v1.2 (1:40, UC Davis/NIH NeuroMab Facility, K14/16), and polyclonal anti-K_v1.1 (1:200, Alomone, APC-009). The monoclonal anti-K_v1.1 antibody binds to endogenous K_v1.1 protein and the anti-K_v1.2 antibody binds to endogenous K_v1.2 protein from rabbit brain membranes, each showing a single band with predicted molecular weight in Western blots (Vacher et al., 2007, Yang et al., 2007). The specific recognition of K_v1.1/K_v1.2 proteins by K36/15 or K14/16 antibody was confirmed by using $K_v1.1^{-/-}$ or $K_v1.2^{-/-}$ mice which serve as negative controls (Lorincz and Nusser, 2008). The polyclonal anti-K_v1.1 antibody, used in our previous studies (Adamson et al., 2002a, Adamson et al., 2002b), showed the same staining pattern as its monoclonal counterpart.

Electrophysiology

Electrodes were coated with silicone-elastomer (Sylgard, Dow Corning) and fire polished (Narishige MF-83) just prior to use. Electrode resistances ranged from 4- 6 MΩ (for whole cell recording) or 6-13 MΩ (for single channel recording) in standard pipette and bath solutions. The junction potential between pipette and extracellular solution was nulled by the voltage-offset of the amplifier (Axopatch 200A) right before establishing the seal and was not further corrected. The liquid junction potential between regular internal and bath solution is 5.1 mV. Series resistance was compensated (95% prediction, 85-95% correction and 10μs lag settings) for voltage clamp recordings of I_h and α-DTX sensitive currents. The

series resistance was 14.6 ± 0.6 MΩ (n = 18) after α-DTX treatment and 15.3 ± 1.2 MΩ (n = 10) after the application of Cs^+. Inward sodium currents were blocked by applying 0.2 μM or 1 μM tetrodotoxin (TTX). Leak currents were subtracted to show the outward currents in control and α-DTX conditions but the α-DTX sensitive difference currents (control minus α-DTX) were measured using the non-leak subtracted traces because of a potential for I_h contamination in the leak-subtraction process (Figure 3). The tail currents seen in the leak-subtracted traces (Fig. 3D and 3E) reflect residual, uncompensated whole cell capacitive currents. Current-clamp measurements were made with the I_{fast} circuitry (Magistretti et al., 1998) of the Axopatch 200A amplifier (Molecular Devices). The input resistance was measured from the plateau portion of each sweep (typically from -80 mV to -60 mV where the current-to-voltage relationship is linear). The value reported here (170 ± 8 MΩ, n = 44) was slightly different from our previous measurements at zero-current membrane potential (∼ -60 mV, Mo and Davis, 1997; Adamson et al., 2002b), which reflects a nonlinear current-to-voltage relationship (data not shown). Neuronal voltage threshold was measured precisely with 1 pA resolution at the peak of the just-subthreshold response and its mean variance is less than 0.5 mV.

The standard internal solution used in all of our whole cell recordings and most of our single channel recordings was as follows (in mM): 112 KCl, 2 $MgCl_2$, 0.1 $CaCl_2$, 11 EGTA, and 10 HEPES, 30 KOH, pH 7.5. The bath solution (in mM) was 137 NaCl, 5 KCl, 1.7 $CaCl_2$, 1 $MgCl_2$, 17 glucose, 13 sucrose, and 10 HEPES-NaOH, pH 7.5; 330 mOsm. For selective pharmacological experiments, rapid solution changes were achieved with a micro-perfusion system (Ogata and Tatebayashi, 1991). The reagents were prepared as stock solutions in distilled water and dissolved in the bath solution for application to neurons. The final concentration was 50 or 100 μM for cadmium chloride ($CdCl_2$), 10 mM for tetraethylammonium chloride (TEA-Cl), 0.2 mM for 4-aminopyridine (4-AP), 100 nM for α-dendrotoxin, 5 mM for cesium chloride (CsCl) and 0.2 μM or 1 μM for TTX. The osmolarity was maintained for TEA solution by replacing equimolar NaCl with TEA-Cl. In addition to Cs^+, I_h current blocker ZD7288 was also tested in our studies. However its onset of action is slow relative to Cs^+ (i.e. up to several minutes versus several seconds (Harris and Constanti, 1995) and often associates with unstable resting potential in the spiral ganglion.

A total of 375 recordings were obtained for this study including single-channel, whole-cell voltage and current clamp experiments. An unpublished analysis from Liu and Davis 2007 was incorporated in panel 5C. Recordings were made from neuronal cell somata at room temperature (19–22°C). Data were digitized at 10 kHz with a CED Power 1401 interface in an IBM-compatible personal computer and filtered at 1 or 2 kHz; the programs for data acquisition and analysis were written by Dr. Mark R. Plummer, Rutgers University. Current-clamp recordings were considered acceptable when they met the following criteria: stable membrane potentials, low noise levels, discernible membrane time constant on step current injection, and overshooting action potentials (magnitudes of ≥70 mV measured from the action potential peak to the nadir of the re-polarization). If any of these parameters changed during an experiment, indicating compromised cell health or metabolic failure, the remaining data were not included in the analysis.

Statistical analysis

Two tail Student's unpaired *t*-test was performed in Microsoft Excel to compare two group means. However, when the control and experimental conditions were assessed from the same neuron such as in the pharmacological experiments a paired t-test was used. For regional comparison between base, middle and apex, one-way ANOVA was used followed by Tukey-Kramer post-hoc pairwise analysis. For immunocytochemical experiments, N-way

ANOVA was used with unbalanced design to account for the uneven neuronal number in each culture dish followed by Tukey-Kramer post-hoc pairwise analysis. ANOVA results and mean ± sem (standard error of mean) values were obtained using Matlab (Mathworks). A p-value < 0.05 indicates significant difference.

Resting membrane potential characterization

Cell-attached single channel recordings were used to assess the resting membrane potential non-invasively (Verheugen et al., 1999). In most experiments, standard internal solution (see above) was used to fill the pipette. For consistency and accuracy, we generally limited our resting membrane potential analyses to channels with a mean conductance of 44.3 pS, which were observed routinely in our recordings and most likely reflect K^+ channel activity (Fricker et al., 1999). In order to measure the resting membrane potential we used equimolar K^+ across the membrane to zero the net flow of K^+ current at 0 mV. Thus, the direction of the single channel current solely depends on the pipette voltage and reverses when the pipette voltage equals RMP. The possibility of recording a chloride channel or HCN channel was ruled out based on the unequal [Cl^-] across the membrane or the small conductance of HCN (Simeone et al., 2005). To further assure K^+ selectivity, a K-Gluconate solution (in mM: 112 K-Gluconate, 5 mM EGTA, 10 HEPES, KOH pH to 7.5) in which the only permeable ion is K^+, was used as pipette solution. The results were consistent with those using the KCl solution because the channel conductance on average is similar (43 pS, n = 4 versus 44 pS, n = 145) and the reversal potential difference (-56.52 mV, n =4 compared to -66.37 mV, n = 145) between the two solutions reflect the junction potential difference (-17 mV versus -5 mV). The data together support the identity of the recorded channels as K^+ channels.

Results

Assessments of threshold and its regulation by ion channels were made using whole-cell patch clamp recordings from spiral ganglion neurons in vitro, isolated from both their peripheral and central synaptic targets (Fig. 1A). Finely graded constant current steps were utilized to determine the voltage threshold for firing from 58 current clamp recordings in control (Fig 1B) and pharmacological conditions; contributing to a total of 375 recordings in the overall study. By evaluating the peak voltage level (Fig 1B, dotted line) at just sub-threshold firing we observed that the data set utilized herein to specifically examine ion channel regulation of voltage threshold firmly established a clear threshold heterogeneity in neurons isolated from the base, middle and apex of the cochlea (Fig. 1C) prior to pharmacological treatment. A closer examination of the data also shows that middle neurons displayed the lowest threshold levels followed by apex neurons, while the basal neurons had thresholds that were markedly higher than the other tonotopic regions (Fig. 1C, thick traces highlight overall trends in voltage threshold level). This electrophysiological pattern is consistent with that reported in a previous study using a separate data set (Liu and Davis, 2007), as was the concurrence of graded timing features. The basal neurons, which achieve the highest thresholds, reach peak voltage faster than the middle neurons and the apical neurons reach their peak voltage at the slowest rate. Therefore, the data from control condition recordings, prior to pharmacological treatment, reiterates the observation that non-monotonic voltage thresholds occur simultaneously with graded timing features (Liu and Davis, 2007).

To facilitate the screening process for likely ion channel candidates that could contribute to this heterogeneous and tonotopically non-monotonic pattern of neuronal excitability we first utilized broad spectrum pharmacological blockers of potassium channels, specifically tetraethylammonium (TEA) to block high threshold K_V3 family currents, 4-aminopyridine

(4-AP) to block low threshold non-inactivating currents along with A-type currents (Mathie et al., 1998) and cadmium (Cd) to block all calcium channel currents. The changes in V_θ were analyzed after fast perfusion of each agent through a bath pipette.

As shown in Figure 1 D-F, 0.2 mM 4-AP, in contrast to $CdCl_2$ and TEA, prominently reduced the action potential threshold voltage (Fig. 1D, average change in mV: - 11.57 ± 0.84 mV, n = 29 versus -1.51 ± 0.47 mV, n = 14 and -2.26 ± 0.37 mV, n = 15, $p < 0.01$ for 4-AP). The example recording (Fig. 1E) shows an example of the alteration observed in electrophysiological profile, while group data (Fig. 1F) confirmed that the impact was not limited to any single neuron or specific spiral ganglion location. These pharmacological effects on voltage threshold (Fig. 1D) revealed that high threshold potassium channels, which were blocked by TEA, were not the main factor in V_θ regulation and therefore the V_θ drop observed from 4-AP application may involve low voltage activated potassium channels. We therefore designed our next set of experiments to pinpoint the contribution of low voltage activated potassium channels in the regulation of V_θ.

To further clarify the relevant ion channels that contribute to the large threshold changes associated with the 4-AP application, we used α-dendrotoxin (α-DTX), which specifically blocks the shaker-related potassium channel family $K_v1.1$, $K_v1.2$ and $K_v1.6$ (Harvey, 2001). When 100 nM α-DTX was applied, spontaneous firing patterns replaced the normally quiescent behavior at neuronal resting potential as shown in the example basal neuron (Fig. 2A, stacked sweeps). For the example shown, initial bursts of trains of action potentials after α-DTX application were soon followed by more regular bursting of two to six action potentials and transitioned into firing doublets (Fig. 2A). This spontaneous firing behavior, without current injection, indicated α-DTX either depolarized the RMP or lowered the V_θ. A rising resting potential could be observed in the current clamp trace leading to burst firing, demonstrating an effect of DTX on the RMP (inset, second from the top, Fig. 2A). In addition, V_θ was considerably reduced such that more hyperpolarizing voltages (-90 mV) were required to hold the neurons at a quiescent level in order to measure the post-DTX voltage thresholds (Fig. 2B). As shown in Figure 2C, the α-DTX effects on shaker-related potassium channels were observed in every recorded neuron from all three cochlear locations thus revealing consistent V_θ decreases. Could α-DTX sensitive potassium channels account for the nonlinear distribution pattern in V_θ? If so, then the high threshold, less excitable basal neurons should have more α-DTX-sensitive shaker family potassium channels while the low threshold, more excitable mid-apical neurons should have fewer such channels. When the average threshold change was analyzed for the base, middle and apex regions, we indeed observed the nonlinear relationship with the basal region being most affected by α-DTX (Fig. 2D in mV, base: -25.73 ± 2.04, n = 11; middle: -14.19 ± 1.28, n = 8; apex: -14.86 ± 2.23, n = 7 , $p < 0.01$ for base).

In addition to its effect on threshold regulation, α-DTX treatment also depolarized neuronal resting membrane potential (as shown in Figure 2A). To assess this effect quantitatively, we measured the RMP changes in the presence of at least 0.2 μM TTX which blocks voltage-gated sodium channels and therefore prevents spontaneous firing. TTX on its own has no effect on the resting potential (data not shown). Consistent with the threshold changes, neurons in the base were most affected (9.61 mV ± 0.58 mV, n = 7, Fig. 2E, $p < 0.05$ between base and middle); whereas, the apical and middle neurons were less affected (7.21 ± 0.31 mV, n = 8 and 6.99 ± 0.9 mV, n = 10, respectively).

The nonlinear alteration of both RMP and V_θ by α-DTX would predict that K_v1 currents are enriched in the base relative to the middle and apex regions. These electrophysiological results were extended further using immunocytochemistry to examine the gangliotopic distribution of $K_v1.1$ and $K_v1.2$ ion channels. We immunostained neuronal cultures from

each cochlear region with specific antibodies against $K_v1.1$ and $K_v1.2$ ion channel α-subunits (green, Fig. 3A, B).

We noted that neurons, irrespective of their ganglion location, showed heterogeneous levels of antibody labeling compared to the relatively uniform neuron-specific β-tubulin antibody distribution (red). Despite these local variations, a tonotopic distribution pattern was also evident. As shown in Figure 3A, basal neurons had higher overall anti-$K_v1.1$ antibody luminance levels than neurons isolated from middle and apical regions. A similar distribution was also found for the anti-$K_v1.2$ antibody (Fig. 3B). A quantitative analysis of antibody luminance (see Methods for details) further confirmed the nonlinear distribution for each subunit from four independent immunocytochemical experiments (Fig. 3C). As shown, the immunolabeling of basal neurons is significantly greater than the mid-apical areas for both α-subunit antibodies. The slightly decreased luminance for the anti-$K_v1.1$ antibody in the middle is consistent with the slight threshold reduction in neurons isolated from the middle cochlear region compared to the apical neurons (Fig 2D). Moreover, $K_v1.1$ subunits have a lower threshold of activation than $K_v1.2$ or $K_v1.6$ in a heterologous expression system (Bähring et al., 2004) and thus would be expected to have a greater influence on threshold regulation. Furthermore, these results are in agreement with our prior immunocytochemical studies using adult animal sections that showed similar apex-base differences in K_v1 channel immunolabeling indicating that these findings pertain to the hearing animal (Adamson et al., 2002b). Lastly, these results are consistent with the electrophysiological findings of the differential impact of α-DTX by cochlear region on both RMP and V_θ (Fig. 2), thus suggesting functional K_v1 channels are enriched in the basal area.

To confirm that the tonotopic difference in $K_v1.1$ immunostaining was indicative of functional, surface-expressed ion channels we performed voltage clamp experiments on spiral ganglion neurons to examine α-DTX sensitive currents directly. Since the average voltage threshold was comparable between the middle and apical regions and base and apex showed clear differences in α-DTX regulation we therefore limited the voltage clamp recordings to base and apex. Recordings were made in the presence of TTX to block inward sodium channels and outward currents were measured in response to 480 ms voltage steps from -75 to -15 mV in 5 mV increments from a holding potential of -80 mV. The example basal neuron recording shown in Fig. 3D indeed had larger outward currents (left panel: Fig. 3D) than the example apical neuron recording (Fig. 3E). As expected for low-threshold K_v1 channels, the currents were completely blocked by α-DTX at lower voltage levels (middle panels: Fig. 3D from -75 to -45 mV; 3E from -75 to -30 mV) before the high threshold potassium channels started to activate. The difference currents (right panels: 3D and 3E), which reflect the K_v1 current component, are evidently larger in the base. The individual recordings and group averages for each region (Fig. 3F) showed consistent differences in the K_v1 conductance, measured at the plateau of each step (symbols in blue and red in 3D, 3E) despite the expected neuron-to-neuron variance. As a result, the average magnitude of K_v1 currents measured from a total of 19 recordings (10 for base and 9 for apex) started to show higher values at -50 mV for the base and became significantly larger at and above -35 mV. Thus, these data provide a strong correlation between functional K_v1 currents and their somatic protein levels.

Another indicator of intrinsic excitability is neuronal firing rate. One of the consequences of reduced thresholds in the mid-apical region might be to increase the firing rate at suprathreshold levels. This idea was supported by the dual effects of K_v1 blockade by α-DTX (Fig. 4A) which not only reduced V_θ from the example neuron but also transformed the originally rapidly accommodating (RA) neuron (the maximum number of action potentials fired during a 240 ms duration or APmax <=8, a criterion used in Liu and Davis, 2007) into a slowly accommodating (SA) one (APmax >=11, Fig. 4A). From these results

and our previous experiments showing the impact of α-DTX on suprathreshold firing alone (Mo et al., 2002), rapidly accommodating neurons would be expected to have more K_v1 channels than their slowly accommodating counterparts. Consequently, the potent threshold regulation by K_v1 channels would result in a higher intrinsic V_θ in these K_v1 enriched, rapidly accomodating neurons. To confirm this, a subset of the recordings from Figure 1 that have quantifiable supra-threshold firing were also assessed for accommodation and the average threshold from the rapidly and slowly accommodating neurons were compared in Figure 4B. The slowly accomodating neurons were indeed significantly more sensitive (-52.33 ± 1.39 mV, n = 6) compared to rapidly accommodating neurons (-45.9 ± 0.83 mV, n = 34, $p < 0.01$). We next asked whether the non-monotonic, tonotopic distribution identified for V_θ would be preserved when rapidly and slowly accommodating neurons were separated according to tonotopic location. To power this analysis we incorporated unpublished analysis from Liu and Davis, 2007 into the current data set which increased the total number of recordings from 40 to 170. As shown in Figure 4C, the tonotopic distribution of threshold between the two categories was retained with rapidly accommodating neurons having consistently higher thresholds than slowly accommodating neurons (-43.41 ± 0.69 mV, n = 44 versus -47.76 ± 0.93 mV, n = 6 for base; -47.79 ± 0.58 mV, n = 45 versus -51.28 ± 0.83 mV, n = 20 for middle; -45.33 ± 0.97 mV, n = 26 versus -48.93 ± 0.57 mV, n = 29 for apex, see figure legend for detailed statistical analysis). Overall, the differential levels of K_v1 observed across the ganglion are consistent with the changes in neuronal intrinsic excitability assessed by measurement of V_θ, ionic currents measured in voltage clamp, and accommodation.

In the spiral ganglion, an ohmic relationship exists between R_{in}, ΔV (differential voltage between baseline potential and voltage threshold) and neuronal current threshold ($R^2 = 0.57$ data not shown). Because R_{in} showed little tonotopic variation, the differential distribution of current threshold in the spiral ganglion was determined mainly by the non-uniform distribution of the barrier to firing which is the voltage difference (ΔV). The firing sensitivity gauge of ΔV is set by both the holding potential and V_θ, thus the inter-dependency of the two parameters would impact the outcome of ΔV. To evaluate whether V_θ is influenced by the holding potential, we changed the holding from -80 mV to -60 mV in 5 mV increments and obtained the threshold at each new holding potential level. When recordings with similar thresholds from the three cochlear regions were compared, it was evident that as the holding potentials were depolarized the voltage thresholds were elevated (Fig. 5A, shows threshold responses at five different holding potentials). This finding was highly consistent in individual recordings (symbols with different shapes or outlines), averaged group data (black lines indicating the means with gray backgrounds representing the standard deviation) and between the three cochlear regions (Fig. 5B). An increasing V_θ that rises with holding potential depolarization, which was also observed in peripheral spiral ganglion nerve terminals from acutely explanted Organ of Corti (Rutherford et al., 2012), might be a consequence of either a reduction in available sodium current due to inactivation (Santos-Sacchi, 1993) or an increase in available low threshold K^+ current. Because a change in holding potential produced a concomitant impact on V_θ, neurons with heterogeneous resting potential levels would be expected to have similarly varied threshold levels by the same mechanisms. Due to the importance of RMP in neuronal intrinsic excitability, we examined additional ion channels that could regulate the RMP.

Another class of ion channels with a known impact on RMP is the HCN channel. The resultant hyperpolarization-activated cationic current (I_h) is well characterized in many neuronal types (Robinson and Siegelbaum, 2003), including spiral ganglion neurons (Mo and Davis, 1997, Yi et al., 2010). Notably, in the spiral ganglion, recordings of I_h displayed a wide distribution in their half-maximal voltage activation (Mo and Davis, 1997), thus raising the possibility that they may have different influences on RMPs across neurons.

To test the contribution of I_h on RMP in spiral ganglion neurons we used CsCl (5 mM), which completely blocks I_h (Mo and Davis, 1997). The specificity of CsCl on I_h was confirmed in the current studies within the voltage range from -55 to -160 mV (Figure 5C). The difference currents in control and Cs^+ conditions revealed no outward component from -55mV to -160 mV indicating that the effects of CsCl on RMP (which is well below -55 mV, see Figure 6B) were attributable to I_h current blockade. As shown in the example recording (Fig. 5D), the cell hyperpolarized from -59.7 to -65.7 mV due to I_h block by CsCl. To test whether the drop in V_θ, which was observed in the individual recording (from -42.2 mV to -44.8 mV) and also the group data (Fig. 5D, $p < 0.01$), was affected indirectly by the change in the zero-current holding potential (Fig. 5A) or directly by CsCl, the holding potential was restored to a constant level (-60 or -80 mV). Indeed, under these circumstances the threshold level was not altered (Fig. 5E) thus indicating that I_h itself has a minimal influence on V_θ regulation. The effect of CsCl-induced hyperpolarization of RMP was observed in recordings from all three areas (Fig. 5F, G, Δ = -3.32 ± 0.55 mV, n = 10; -2.74 ± 0.70 mV, n = 8; -3.94 ± 0.83 mV, n = 5 for base, middle and apex neurons, respectively). Because of the relatively small and uniform effects on RMP, the tonotopic pattern of HCN channel subunits was not examined further. Nevertheless, these data indicate that I_h has a functional role on the RMP in spiral ganglion neurons.

For the characterization of V_θ (Figures 1, 2 and 4) we used a constant holding potential of -80 mV (or -90 mV) in an effort to remove steady-state inactivation of depolarization-activated ion channels such as sodium or low threshold potassium channels. However, it is equally important to know the endogenous RMP of spiral ganglion neurons and examine how V_θ or ΔV is affected by holding a cell at its endogenous resting potential. Thus in our next experiments, a single channel recording was used to non-invasively assess the intracellular RMP (see Methods, Fig 6A inset) and then the neuronal threshold and ΔV was measured by holding the cell at that specific RMP level (Fig. 7).

As shown in Figure 6, three current-to-voltage relationships obtained from example single channel recordings for apex, middle and base, despite having similar conductances (44, 43, 42 pS from base to apex), revealed a nonlinear distribution in the calculated RMP. The mid-apical neurons had the most depolarized resting potentials whereas basal neurons had the most hyperpolarized resting potentials (Fig. 6A, from base to apex, in mV, -67.86, -63.19 and -63.75). The group data confirmed such a nonlinear pattern when RMPs were averaged from all single channel recordings obtained from each area (Fig. 6B, -68.7 ± 0.55 mV, n = 24; -65.26 ± 0.66 mV, n = 26; -65.54 ± 0.66 mV, n = 23 for base, middle and apex neurons, respectively; $p < 0.01$ for base). When the RMP was evaluated within 30 seconds of switching to whole-cell current clamp mode, we observed similar, though slightly depolarized, values (Fig. 6C, -64.27 ± 1.18 mV, n = 12; -59.09 ± 0.94 mV, n = 8; -58.85 ± 1.33 mV, n = 10 from base to apex; $p < 0.01$ for base). This series of experiments demonstrate that endogenous RMP showed a distribution that mirrored V_θ.

To assess firing sensitivity closer to the neuronal physiological state we first calculated the endogenous RMP as described above, matched the holding potential to the calculated RMP and then assessed the voltage threshold. To depict the endogenous distribution of V_θ and RMP, current clamp traces at threshold were overlaid for the basal, middle and apical regions in Figure 7A. When the endogenous RMP was used as the holding potential there was a substantial heterogeneity in threshold that was widest in the basal region. Consistent with our earlier set of experiments using the same single channel technique, the basal region also had the most hyperpolarized average endogenous RMP (in mV, -67.6 ± 0.7, n = 32; -65.41 ± 0.47, n = 38; -65.45 ± 0.44, n = 30 from base to apex, $p < 0.01$ for base). Thresholds (within the range emphasized by the thick black lines in Figure 7A), were significantly higher for the basal neurons (Fig. 7B, $p < 0.01$), despite the wider range and

more hyperpolarized resting potentials. Moreover, mean V_θ was comparable in the apical and middle regions when holding neurons at their endogenous RMPs (Fig. 7B).

Would the heterogeneity in V_θ be affected by holding the neurons at different RMPs? As shown in Figure 7C, three separate recordings obtained from the middle region displayed widely different thresholds despite being held at similar baseline levels. When V_θ and RMP are taken together, what emerges is that threshold heterogeneity is retained in every cochlear region especially from neurons with similar RMPs (Fig. 7D). Further, the differential voltage is emphasized by connecting equal values at two intermediate levels (20 and 30 mV lines, Fig. 7D). The basal neurons have differential voltage magnitudes that were almost all above 20 mV, and many above 30 mV, whereas the middle and apical neurons had mixed distributions with many below the 20 mV level. By comparing the differential voltage that takes both resting potential and threshold voltage into account, what emerges is that basal neurons are generally less excitable compared to their middle and apical couterparts.

Discussion

Heterogeneity is a prominent feature within the organ of Corti. For example, the presynaptic morphology of ribbon synapses within a single hair cell displays different shapes and sizes (Merchan-Perez and Liberman, 1996, Meyer et al., 2009, Liberman et al., 2011, Wong et al., 2013), while the post-synaptic terminals of spiral ganglion neurons possess AMPA receptor patches displaying opposing size gradients to their pre-synaptic partners (Liberman et al., 2011). Moreover, electrophysiological studies from the somata of spiral ganglion neurons also revealed an additional level of heterogeneity in their firing features (Mo and Davis, 1997, Adamson et al., 2002b, Reid et al., 2004, Liu and Davis, 2007), the greatest of which is the intrinsic excitability set by the combination of resting potential and threshold level within each cochlear region examined. Some or all of these well-characterized features are most likely important, in part, to tailor input within a divergent pathway formed by the multiple type I spiral ganglion neurons that establish one-to-one synaptic connections with a single inner hair cell.

In contrast to a system, such as crustacean stomatogastric ganglion, where heterogeneous intrinsic excitability could serve to counterbalance the diverse synaptic input and maintain a homeostatic output (Schulz, 2006, Misonou, 2010), auditory neurons have a heterogeneous output function with diverse spontaneous and sound activated discharge patterns (Taberner and Liberman, 2005). Therefore, promoting a diversity of neuronal intrinsic excitability through ionic mechanisms would strengthen, rather than attenuate, heterogeneous neural behavior. Similar strategies have been used in many parts of the nervous systems including periglomerular cells in the olfactory bulb (Puopolo and Belluzzi, 1998), primary nociceptive neurons (Gascon and Moqrich, 2010), and dorsal cochlear nucleus pyramidal neurons (Leao et al., 2012). Functionally, a heterogeneous neuronal population can enhance the dynamic range of a system (Angelo and Margrie, 2011), as well as improve coding efficiency for cells processing different aspects of sensory stimuli (Marsat and Maler, 2010). For example, the diversity of primary nociceptive neurons enables coding of noxious input from many different sources (Gascon and Moqrich, 2010), while heterogeneous populations of mitral cells of the mouse olfactory bulb are capable of encoding more odorant information than a homogeneous group (Padmanabhan and Urban, 2010).

Our studies revealed a set of mechanisms for the establishment of a heterogeneous neuronal intrinsic excitability profile. We therefore expect spiral ganglion neurons even from the same cochlear region to possess a mixture of current magnitudes carried by K_v1 and HCN channels to establish a specific threshold and RMP set value. The differential combination is critical for these neurons to maintain a physiological threshold range of 30 mV (from ∼-60

to -30 mV) and resting potential range of 20 mV (from -55 to -75 mV). Not only do these mechanisms explain the local heterogeneity in the sub-threshold voltage range prior to firing, but also set the base spiral ganglion neurons apart, which had the largest K_v1 current amplitudes and differential voltage range from resting to threshold. Thus, for a neuron that must couple a high threshold level with a low resting membrane potential, the inclusion of additional functional K_v1 channels can exert both effects simultaneously (Figure 8A, yellow arrow). However, additional resting potential regulation is necessary to decouple the threshold and resting potential changes. For example, to prevent neurons with low thresholds from spontaneous firing (Figure 8A, B, lower right), inclusion of fewer HCN channels (Figure 8A, magenta arrow) or other mechanisms (such as more chloride or leak channels (Chen and Davis 2006) or enhanced Na^+/K^+-ATPase activity (Kim et al. 2007), are required (Figure 8A, blue arrow). On the other hand, the lack of correlation between highest thresholds and most hyperpolarized resting potentials may suggest K_v1 has limited impact on RMP when the resting potential goes below the K_v1 activation voltage.

We also found that in contrast to K_v1 channel regulation, threshold and resting potential were passively linked in opposite directions, such that higher resting potentials lead to higher thresholds (Figure 8A and Figure 5B, line and shadow plot). This mechanism is important to maintain a stable neuronal sub-threshold range when neuronal resting potential changes during activity. To complete the full picture, other factors such as the impact of myelination on ion channel distribution could also contribute but were not explored herein, while the maximal level of sodium current magnitude was not found to be significantly different between the apical and basal neurons (unpublished observations).

Similar ionic control through K_v1 channels was found to regulate the heterogeneity of intrinsic excitability in other cell types. For example, $K_v1.1$ channels underlie the firing of high threshold but not low threshold C-mechano-nociceptors nerve fibers (Hao et al., 2013). This is in contrast to other mechanisms of intrinsic excitability regulation. For example, modification of inward rectifier potassium currents varied the resting potential of DCN principal neurons from -60 to -70 mV which allowed for transitions between spontaneously active and non-active states by activating subthreshold persistent sodium channels above but not below -65 mV (Leao et al., 2012).

Impact of intrinsic excitability on neuronal output

Our findings on spiral ganglion neurons, without their hair cell contacts, show the expected positive relationship between neuronal intrinsic excitability and firing rate such that low threshold neurons tend to fire more. This functional correlation is consistent with that observed *in vivo*, with low threshold fibers having higher spontaneous discharge rates than high threshold fibers (Taberner and Liberman, 2005). Our studies indicate that an important ionic regulator of these two key features could be K_v1, one function of which would be to act as a general substrate to regulate neuronal intrinsic excitability through accommodation, as well as threshold level and RMP, as observed in numerous neuronal cell types (Brew and Forsythe, 1995, Mo et al., 2002, Lopantsev et al., 2003, Chi and Nicol, 2007).

In addition to having a direct influence on voltage threshold levels, resting membrane potential can also change neuronal firing patterns. For example, altered neuronal membrane potential abolished rebound burst firing in thalamocortical neurons (Kim and McCormick, 1998). In spiral ganglion neurons, the regulation of holding potential on neuronal output was also observed in a subset of rapidly accommodating neurons that could be transformed into slowly accommodating neurons with a change of holding potential (from -80 to -60 mV, Crozier and Davis, 2013).

Potential contribution of heterogeneous excitability to fine-tuning of neural-sensory circuit during development

Afferent type I nerve fibers only synapse onto one IHC but each IHC is innervated by multiple nerve fibers. Anatomically, high threshold, low to medium spontaneous discharge rate (SR) fibers contact the modiolar surface of the IHCs whereas low threshold, high SR fibers contact the pillar surface (Liberman, 1982), but it is unclear how such a rich innervation and spatial segregation pattern is achieved. It is currently postulated that the proper wiring relies on postsynaptic signals, as the convergence of the nerve fibers onto the same sources of IHCs was shown not to require pre-synaptic Ca^{2+} activity or neurotransmitter release from the IHC (Bulankina and Moser, 2012) and Gata3, a transcription factor expressed in the spiral ganglion, regulates the proper innervation pattern (Appler et al., 2013). It is also possible that changes in spiral ganglion neuronal intrinsic excitability participate in the proper wiring of nerve fibers, similar to that found in the neocortex where altered neuronal intrinsic excitability was associated with changes in microcircuit connectivity (Rinaldi et al., 2008). To address whether Gata3 regulation of spiral ganglion wiring alters ion channel composition predictably, it would be valuable to know whether altered intrinsic excitability occurs in tandem with improper spiral ganglion wiring.

The endogenous properties of spiral ganglion neurons in explant cultures undergo dramatic changes in intrinsic excitability during the first 2 weeks prior to hearing onset (Crozier and Davis, 2013). The majority of changes in excitability stabilize by postnatal day 4 (P4) such that spiral ganglion neurons from P14 animals retain both regional as well as tonotopic characteristics of voltage thresholds presented herein (Crozier and Davis, 2013). In addition, evidence from our laboratory indicates that K_v1 channel distribution, among other important regulators of spiral ganglion neuron function such as the tonotopic gradient of neurotrophin-3, AMPA receptor distribution, and other potassium channels, are expressed with similar tonotopic trends in adult animals as postnatal animals when assessed with immunocytochemistry (Adamson et al., 2002b, Flores-Otero and Davis, 2011). Therefore, our results from pre-hearing animials may extend to the hearing animal, as well.

Potential contribution of heterogeneous excitability to diverse in vivo thresholds

The rich innervation of a single IHC by many nerve fibers with different threshold levels provided early evidence that functionally distinct pathways are present to convey intensity in addition to frequency information (Liberman, 1982). It is unclear why the nerve fibers are activated at different sound levels. Several stages during the signal transmission from the periphery could participate. For example, calcium signaling within IHCs are required to trigger afferent neurotransmitter release and subsequent activation of postsynaptic AMPA receptors (Glowatzki et al., 2008). The resulting excitatory postsynaptic potentials (EPSPs) then overcome the neuronal terminal threshold (Glowatzki and Fuchs, 2002, Yi et al., 2010, Rutherford et al., 2012) to initiate spikes at the heminode close to the foramina nervosa (Hossain et al., 2005) which then travel along a myelinated neuronal process and through a bipolar shaped cell soma before reaching the central axonal segment where it is recorded in single unit studies (Liberman, 1982).

Could heterogeneous spiral ganglion neuron intrinsic excitability combine with the upstream synaptic input to differentiate the nerve fiber thresholds? It is possible that the low threshold, high SR fibers have larger pre-synaptic Ca^{2+} influx (Wong et al., 2013) or postsynaptic AMPA receptor patch sizes (Liberman et al., 2011) which, when fully activated, would provide more synaptic driving force. Increased driving force coupled with a lower intrinsic firing threshold at the terminal or cell soma might further enhance the discharge of the nerve

fibers, and future studies are needed to determine whether the high SR fibers have reduced intrinsic thresholds.

Besides their roles in direct regulation of intrinsic excitability at the soma, the expression of I_h (Yi et al., 2010) or K_v1 channels (Mathews et al., 2010) located in the processes of peripheral or central auditory neurons, respectively, would abbreviate the decay and reduce the temporal summation of EPSPs. Consistent with the contribution to neuronal timing, a noticeable delay in action potential latency was observed in our pharmacological studies when K_v1 was blocked. A reduction in temporal summation would negatively impact nerve terminal firing to sub-threshold EPSP events. This may be especially important for intensity coding because paired whole-cell recordings from a hair cell coupled to a synaptic bouton demonstrated a stable average magnitude but more frequent EPSC events in response to increased pre-synaptic hair cell depolarization (Goutman and Glowatzki, 2007, Li et al., 2009).

In summary, our studies suggest that spiral ganglion neurons possess a diverse neuronal output through ionic control of their intrinsic excitability. It is noteworthy that these diverse intrinsic states are measured from neurons isolated from their synaptic targets and thus are not spontaneously active nor do they receive synaptic input or efferent feedback. Interestingly the nerve fibers in vivo also exhibit heterogeneous thresholds. Recent studies suggest, however, these in vitro or in vivo measurements may only represent one aspect of neuronal function because the nerve fibers naturally adapt their in vivo thresholds to track the changes in the mean sound levels of more complex sounds (Wen et al., 2009). One indication that the dynamic regulation of a single fiber baseline threshold level depends upon synaptic mechanisms is the rapid AMPA receptor regulation observed in vivo (Chen et al., 2007). It is also possible that ion channels such as K_v1 undergo rapid phosphorylation similar to that of K_v3 channels observed in vivo (Song et al., 2005). Future studies are required to determine whether an instant modification of the ion channels by sound stimulation can complement the more chronic control observed from neurotrophic factors (Zhou et al., 2005) to enhance spiral ganglion neuron coding capacity to dynamic sound input.

Acknowledgments

We thank Dr. Mark R. Plummer and Dr. Robert Crozier for discussions and critical reading of the manuscript and Huizhong (Susan) Xue for expert technical support. The work is supported by NIH NIDCD RO1 DC01856.

References

Adamson CL, Reid MA, Davis RL. Opposite actions of brain-derived neurotrophic factor and neurotrophin-3 on firing features and ion channel composition of murine spiral ganglion neurons. J Neurosci. 2002a; 22:1385–1396. [PubMed: 11850465]

Adamson CL, Reid MA, Mo ZL, Bowne-English J, Davis RL. Firing features and potassium channel content of murine spiral ganglion neurons vary with cochlear location. J Comp Neurol. 2002b; 447:331–350. [PubMed: 11992520]

Angelo K, Margrie TW. Population diversity and function of hyperpolarization-activated current in olfactory bulb mitral cells. Sci Rep. 2011; 1

Appler JM, Lu CC, Druckenbrod NR, Yu WM, Koundakjian EJ, Goodrich LV. Gata3 is a critical regulator of cochlear wiring. J Neurosci. 2013; 33:3679–3691. [PubMed: 23426694]

Bähring R, Vardanyan V, Pongs O. Differential modulation of Kv1 channel-mediated currents by co-expression of Kvbeta3 subunit in a mammalian cell-line. Mol Membr Biol. 2004; 21:19–25. [PubMed: 14668135]

Brew HM, Forsythe ID. Two voltage-dependent K+ conductances with complementary functions in postsynaptic integration at a central auditory synapse. J Neurosci. 1995; 15:8011–8022. [PubMed: 8613738]

Bulankina AV, Moser T. Neural circuit development in the mammalian cochlea. Physiology (Bethesda). 2012; 27:100–112. [PubMed: 22505666]

Chen Z, Kujawa SG, Sewell WF. Auditory sensitivity regulation via rapid changes in expression of surface AMPA receptors. Nat Neurosci. 2007; 10:1238–1240. [PubMed: 17828255]

Chi XX, Nicol GD. Manipulation of the Potassium Channel Kv1.1 and Its Effect on Neuronal Excitability in Rat Sensory Neurons. J Neurophysiol. 2007; 98:2683–2692. [PubMed: 17855588]

Corwin JT, Warchol ME. Auditory hair cells: structure, function, development, and regeneration. Annu Rev Neurosci. 1991; 14:301–333. [PubMed: 2031573]

Crozier R, Davis RL. Development of Spiral Ganglion Neuron Intrinsic Excitability and Modulation by NT-3 in CBA Mice Abstracts of the Association of Research for Otolaryngology. 2013; 36:904.

Davis RL, Liu Q. Complex primary afferents: What the distribution of electrophysiologically-relevant phenotypes within the spiral ganglion tells us about peripheral neural coding. Hear Res. 2011; 276:34–43. [PubMed: 21276843]

Echteler SM, Nofsinger YC. Development of ganglion cell topography in the postnatal cochlea. J Comp Neurol. 2000; 425:436–446. [PubMed: 10972943]

Flores-Otero J, Davis RL. Synaptic proteins are tonotopically graded in postnatal and adult type I and type II spiral ganglion neurons. J Comp Neurol. 2011; 519:1455–1475. [PubMed: 21452215]

Fricker D, Verheugen JAH, Miles R. Cell-attached measurements of the firing threshold of rat hippocampal neurones. J Physiol. 1999; 517:791–804. [PubMed: 10358119]

Gascon E, Moqrich A. Heterogeneity in primary nociceptive neurons: From molecules to pathology. Arch Pharm Res. 2010; 33:1489–1507. [PubMed: 21052929]

Glowatzki E, Fuchs PA. Transmitter release at the hair cell ribbon synapse. Nat Neurosci. 2002; 5:147–154. [PubMed: 11802170]

Glowatzki E, Grant L, Fuchs P. Hair cell afferent synapses. Curr Opin Neurobiol. 2008; 18:389–395. [PubMed: 18824101]

Goutman JD, Glowatzki E. Time course and calcium dependence of transmitter release at a single ribbon synapse. Proc Natl Acad Sci U S A. 2007; 104:16341–16346. [PubMed: 17911259]

Hao J, Padilla F, Dandonneau M, Lavebratt C, Lesage F, Noël J, Delmas P. Kv1.1 channels act as mechanical brake in the senses of touch and pain. Neuron. 2013; 77:899–914. [PubMed: 23473320]

Harris NC, Constanti A. Mechanism of block by ZD 7288 of the hyperpolarization-activated inward rectifying current in guinea pig substantia nigra neurons in vitro. J Neurophysiol. 1995; 74:2366–2378. [PubMed: 8747199]

Harvey AL. Twenty years of dendrotoxins. Toxicon. 2001; 39:15–26. [PubMed: 10936620]

Hossain WA, Antic SD, Yang Y, Rasband MN, Morest DK. Where is the spike generator of the cochlear nerve? Voltage-gated sodium channels in the mouse cochlea. J Neurosci. 2005; 25:6857–6868. [PubMed: 16033895]

Kim JH, Sizov I, Dobretsov M, von Gersdorff H. Presynaptic Ca2+ buffers control the strength of a fast post-tetanic hyperpolarization mediated by the alpha3 Na(+)/K(+)- ATPase. Nat Neurosci. 2007; 10:196–205. [PubMed: 17220883]

Kim U, McCormick DA. The Functional Influence of Burst and Tonic Firing Mode on Synaptic Interactions in the Thalamus. J Neurosci. 1998; 18:9500–9516. [PubMed: 9801387]

Kim YH, Chung S, Lee YH, Kim EC, Ahn DS. Increase of L-type Ca2+ current by protease-activated receptor 2 activation contributes to augmentation of spontaneous uterine contractility in pregnant rats. Biochem Biophys Res Commun. 2012; 418:167–172. [PubMed: 22244874]

Leao RM, Li S, Doiron B, Tzounopoulos T. Diverse levels of an inwardly rectifying potassium conductance generate heterogeneous neuronal behavior in a population of dorsal cochlear nucleus pyramidal neurons. J Neurophysiol. 2012; 107:3008–3019. [PubMed: 22378165]

Li GL, Keen E, Andor-Ardó D, Hudspeth AJ, von Gersdorff H. The unitary event underlying multiquantal EPSCs at a hair cell's ribbon synapse. J Neurosci. 2009; 29:7558–7568. [PubMed: 19515924]

Liberman LD, Wang H, Liberman MC. Opposing gradients of ribbon size and AMPA receptor expression underlie sensitivity differences among cochlear-nerve/hair-cell synapses. J Neurosci. 2011; 31:801–808. [PubMed: 21248103]

Liberman MC. Single-neuron labeling in the cat auditory nerve. Science. 1982; 216:1239–1241. [PubMed: 7079757]

Liberman MC, Oliver ME. Morphometry of intracellularly labeled neurons of the auditory nerve: correlations with functional properties. J Comp Neurol. 1984; 223:163–176. [PubMed: 6200517]

Liu Q, Davis RL. Regional Specification of Threshold Sensitivity and Response Time in CBA/CaJ Mouse Spiral Ganglion Neurons. J Neurophysiol. 2007; 98:2215–2222. [PubMed: 17715200]

Lopantsev V, Tempel BL, Schwartzkroin PA. Hyperexcitability of CA3 Pyramidal Cells in Mice Lacking the Potassium Channel Subunit Kv1.1. Epilepsia. 2003; 44:1506–1512. [PubMed: 14636320]

Lorincz A, Nusser Z. Cell-Type-Dependent Molecular Composition of the Axon Initial Segment. J Neurosci. 2008; 28:14329–14340. [PubMed: 19118165]

Magistretti J, Mantegazza M, de Curtis M, Wanke E. Modalities of distortion of physiological voltage signals by patch-clamp amplifiers: a modeling study. Biophys J. 1998; 74:831–842. [PubMed: 9533695]

Marsat G, Maler L. Neural heterogeneity and efficient population codes for communication signals. J Neurophysiol. 2010; 104:2543–2555. [PubMed: 20631220]

Mathews PJ, Jercog PE, Rinzel J, Scott LL, Golding NL. Control of submillisecond synaptic timing in binaural coincidence detectors by K(v)1 channels. Nat Neurosci. 2010; 13:601–609. [PubMed: 20364143]

Mathie A, Wooltorton JR, Watkins CS. Voltage-activated potassium channels in mammalian neurons and their block by novel pharmacological agents. Gen Pharmacol. 1998; 30:13–24. [PubMed: 9457476]

Merchan-Perez A, Liberman MC. Ultrastructural differences among afferent synapses on cochlear hair cells: correlations with spontaneous discharge rate. J Comp Neurol. 1996; 371:208–221. [PubMed: 8835727]

Meyer AC, Frank T, Khimich D, Hoch G, Riedel D, Chapochnikov NM, Yarin YM, Harke B, Hell SW, Egner A, Moser T. Tuning of synapse number, structure and function in the cochlea. Nat Neurosci. 2009; 12:444–453. [PubMed: 19270686]

Misonou H. Homeostatic regulation of neuronal excitability by K(+) channels in normal and diseased brains. Neuroscientist. 2010; 16:51–64. [PubMed: 20236949]

Mo ZL, Adamson CL, Davis RL. Dendrotoxin-sensitive K+ currents contribute to accommodation in murine spiral ganglion neurons. J Physiol. 2002; 542:763–778. [PubMed: 12154177]

Mo ZL, Davis RL. Heterogeneous voltage dependence of inward rectifier currents in spiral ganglion neurons. J Neurophysiol. 1997; 78:3019–3027. [PubMed: 9405521]

Nadol JB Jr, Burgess BJ, Reisser C. Morphometric analysis of normal human spiral ganglion cells. Ann Otol Rhinol Laryngol. 1990; 99:340–348. [PubMed: 2337313]

Ogata N, Tatebayashi H. A simple and multi-purpose “concentration-clamp” method for rapid superfusion. J Neurosci Methods. 1991; 39:175–183. [PubMed: 1724682]

Padmanabhan K, Urban NN. Intrinsic biophysical diversity decorrelates neuronal firing while increasing information content. Nat Neurosci. 2010; 13:1276–1282. [PubMed: 20802489]

Puopolo M, Belluzzi O. Functional heterogeneity of periglomerular cells in the rat olfactory bulb. Eur J Neurosci. 1998; 10:1073–1083. [PubMed: 9753175]

Raphael Y, Altschuler RA. Structure and innervation of the cochlea. Brain Res Bull. 2003; 60:397–422. [PubMed: 12787864]

Reid MA, Flores-Otero J, Davis RL. Firing patterns of type II spiral ganglion neurons in vitro. J Neurosci. 2004; 24:733–742. [PubMed: 14736859]

Rinaldi T, Silberberg G, Markram H. Hyperconnectivity of Local Neocortical Microcircuitry Induced by Prenatal Exposure to Valproic Acid. Cereb Cortex. 2008; 18:763–770. [PubMed: 17638926]

Robinson RB, Siegelbaum SA. Hyperpolarization-activation cation currents: from molecules to physiological function. Annu Rev Physiol. 2003; 65:453–480. [PubMed: 12471170]

Rosbe KW, Burgess BJ, Glynn RJ, Nadol JB Jr. Morphologic evidence for three cell types in the human spiral ganglion. Hear Res. 1996; 93:120–127. [PubMed: 8735073]

Rutherford MA, Chapochnikov NM, Moser T. Spike Encoding of Neurotransmitter Release Timing by Spiral Ganglion Neurons of the Cochlea. J Neurosci. 2012; 32:4773–4789. [PubMed: 22492033]

Ryugo, DK. The auditory nerve: peripheral innervation cell body morphology, and central projections. In: Webster, DB., et al., editors. The Mammalian Auditory Pathway: Neuroanatomy. New York: Springer-Verlag; 1992. p. 23-65.

Santos-Sacchi J. Voltage-dependent ionic conductances of type I spiral ganglion cells from the guinea pig inner ear. J Neurosci. 1993; 13:3599–3611. [PubMed: 8393487]

Schulz DJ. Plasticity and stability in neuronal output via changes in intrinsic excitability: it's what's inside that counts. J Exp Biol. 2006; 209:4821–4827. [PubMed: 17142671]

Simeone TA, Rho JM, Baram TZ. Single channel properties of hyperpolarization-activated cation currents in acutely dissociated rat hippocampal neurones. J Physiol. 2005; 568:371–380. [PubMed: 16123099]

Song P, Yang Y, Barnes-Davies M, Bhattacharjee A, Hamann M, Forsythe ID, Oliver DL, Kaczmarek LK. Acoustic environment determines phosphorylation state of the Kv3.1 potassium channel in auditory neurons. Nat Neurosci. 2005; 8:1335–1342. [PubMed: 16136041]

Sun W, Salvi RJ. Brain derived neurotrophic factor and neurotrophic factor 3 modulate neurotransmitter receptor expressions on developing spiral ganglion neurons. Neuroscience. 2009; 164:1854–1866. [PubMed: 19778585]

Taberner AM, Liberman MC. Response properties of single auditory nerve fibers in the mouse. J Neurophysiol. 2005; 93:557–569. [PubMed: 15456804]

Vacher H, Mohapatra DP, Misonou H, Trimmer JS. Regulation of Kv1 channel trafficking by the mamba snake neurotoxin dendrotoxin K. FASEB J. 2007; 21:906–914. [PubMed: 17185748]

Verheugen JA, Fricker D, Miles R. Noninvasive measurements of the membrane potential and GABAergic action in hippocampal interneurons. J Neurosci. 1999; 19:2546–2555. [PubMed: 10087068]

Wen B, Wang GI, Dean I, Delgutte B. Dynamic range adaptation to sound level statistics in the auditory nerve. J Neurosci. 2009; 29:13797–13808. [PubMed: 19889991]

Wong AB, Jing Z, Rutherford MA, Frank T, Strenzke N, Moser T. Concurrent Maturation of Inner Hair Cell Synaptic Ca2+ Influx and Auditory Nerve Spontaneous Activity around Hearing Onset in Mice. J Neurosci. 2013; 33:10661–10666. [PubMed: 23804089]

Yang JW, Vacher H, Park KS, Clark E, Trimmer JS. Trafficking-dependent phosphorylation of Kv1.2 regulates voltage-gated potassium channel cell surface expression. Proc Natl Acad Sci U S A. 2007; 104:20055–20060. [PubMed: 18056633]

Yi E, Roux I, Glowatzki E. Dendritic HCN channels shape excitatory postsynaptic potentials at the inner hair cell afferent synapse in the mammalian cochlea. J Neurophysiol. 2010; 103:2532–2543. [PubMed: 20220080]

Zhou Z, Liu Q, Davis RL. Complex regulation of spiral ganglion neuron firing patterns by neurotrophin-3. J Neurosci. 2005; 25:7558–7566. [PubMed: 16107643]

Abbreviations

IHC	inner hair cell
RMP	resting membrane potential
V_θ	voltage threshold
HCN	hyperpolarization-activated cationic channel

SR	spontaneous discharge rate
EPSP	excitatory postsynaptic potential
DTX	dendrotoxin
TTX	tetrodotoxin
4-AP	4-aminopyridine
TEA	tetraethylammonium

Highlights

- SGN excitability determined by V_θ and RMP is heterogeneous, varying tonotopically.
- RMP mirrored tonotopic V_θ distribution to enhance SGN heterogeneity.
- K_v1 channels affect both RMP and V_θ, whereas HCN channels primarily impact RMP.
- Multiple elements, including K_v1 and HCN channels, regulate SGN excitability.
- Heterogeneous excitability can have broad-reaching effects in sensory systems.

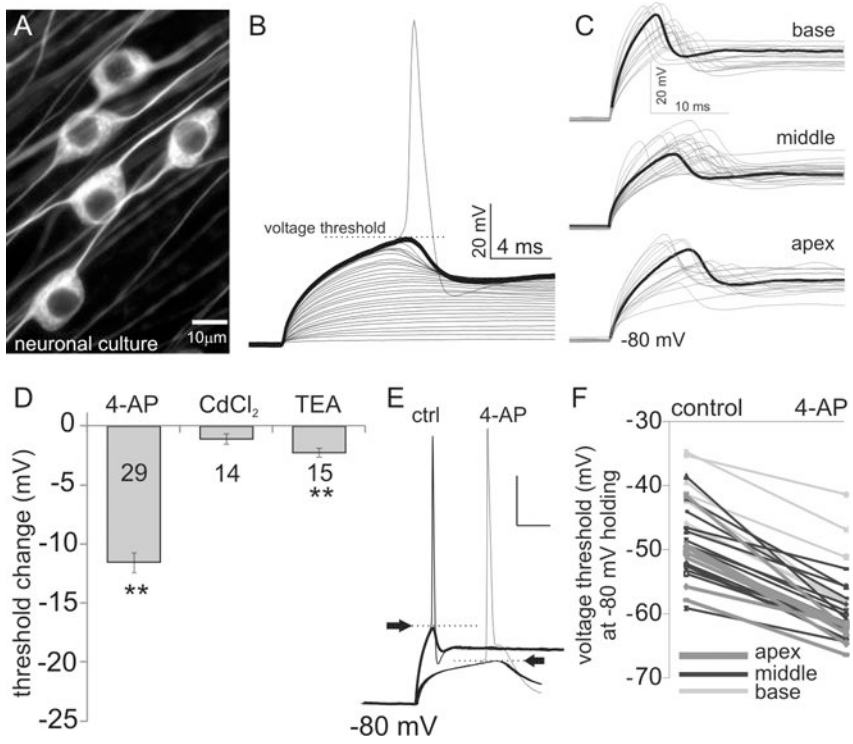

Fig. 1.

Mid-apical spiral ganglion neurons have the most sensitive firing thresholds, which are altered by 4-AP. (A) An example of a neuronal culture stained with the neuron-specific marker β-III-tubulin highlighting the bipolar morphology of these cells. (B) A stack of whole-cell current clamp traces from one example recording illustrate neuronal responses up to threshold with step current injections. (C) Overlays of just sub-threshold current clamp traces from neuronal cultures dissociated from basal, middle and apical cochlear regions showed heterogeneous voltage thresholds at a holding potential of -80 mV. The thick black traces highlight the distinctive trends in threshold and kinetics along the ganglion. (D) Comparison of average threshold change by 0.2 mM 4-AP, 50 or 100 μM $CdCl_2$ and 10 mM TEA. **: $p<0.01$, two-tail paired Student's *t*-test. Number of recordings is shown in each bar for this and subsequent figures. (E) Example current clamp recordings at threshold (with action potentials) and just sub-threshold response levels before (left) and after (right) the perfusion of 4-AP. Arrows indicate threshold levels for this and subsequent figures. Scale bar: 20 mV by 25 ms. (F) Pair-wise comparison of neuronal threshold before and after the application of 0.2 mM 4-AP. Gray scale for this and subsequent figures indicate the location of recordings: light grey for base; black for middle and dark grey for apex.

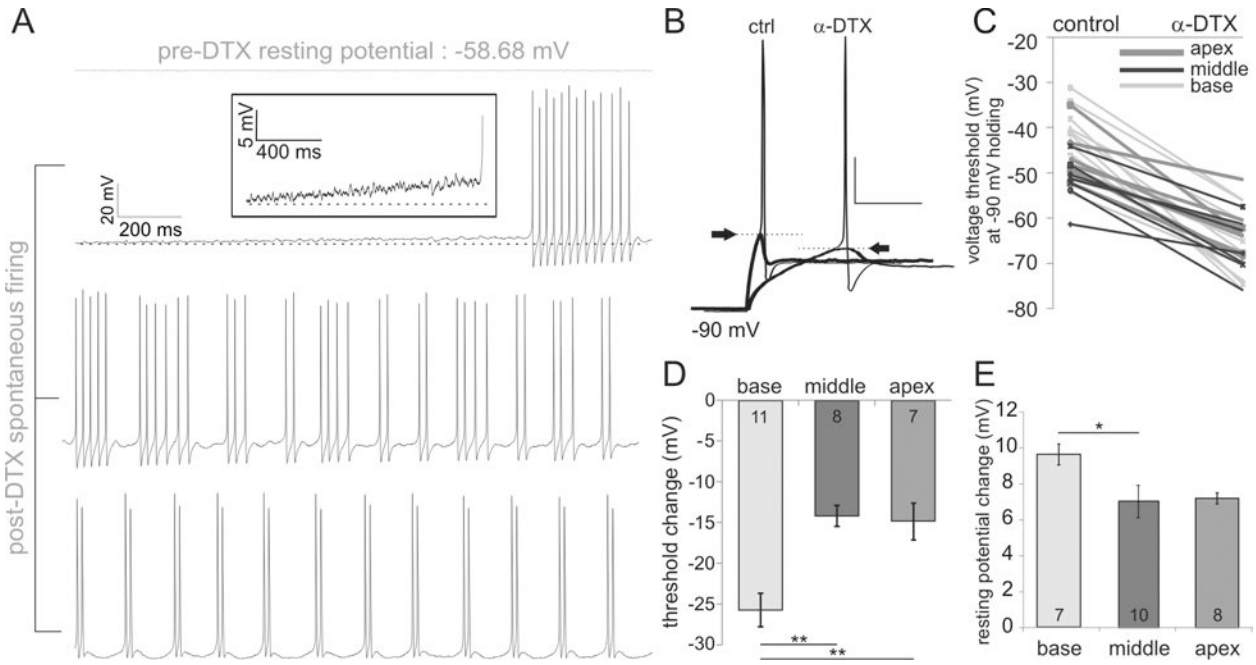

Fig. 2.

The specific blocker of K_v1 ion channels, α-DTX, has a dual impact on intrinsic excitability by lowering voltage threshold and depolarizing resting potential. (A) Quiescent resting membrane potential prior to α-DTX treatment was replaced by spontaneous activity from an example basal spiral ganglion neuron (stacked traces, top to bottom in chronological order) after 100 nM α-DTX treatment. References to dotted horizontal lines highlight the change in resting potential. Inset in the upper left panel shows the depolarizing baseline at higher gain. (B) Current clamp recordings at threshold (with action potentials) and just sub-threshold from one basal neuron before (left) and after (right) perfusion of 100 nM α-DTX. . Scale bar: 20 mV by 25 ms. Holding potential was set to -90 mV to accommodate the threshold drop. (C) Pair-wise comparison of neuronal thresholds before and after the application of 100 nM α-DTX. (D-E) Changes in threshold (D) or resting membrane potential (E) from base to apex after α-DTX treatment.

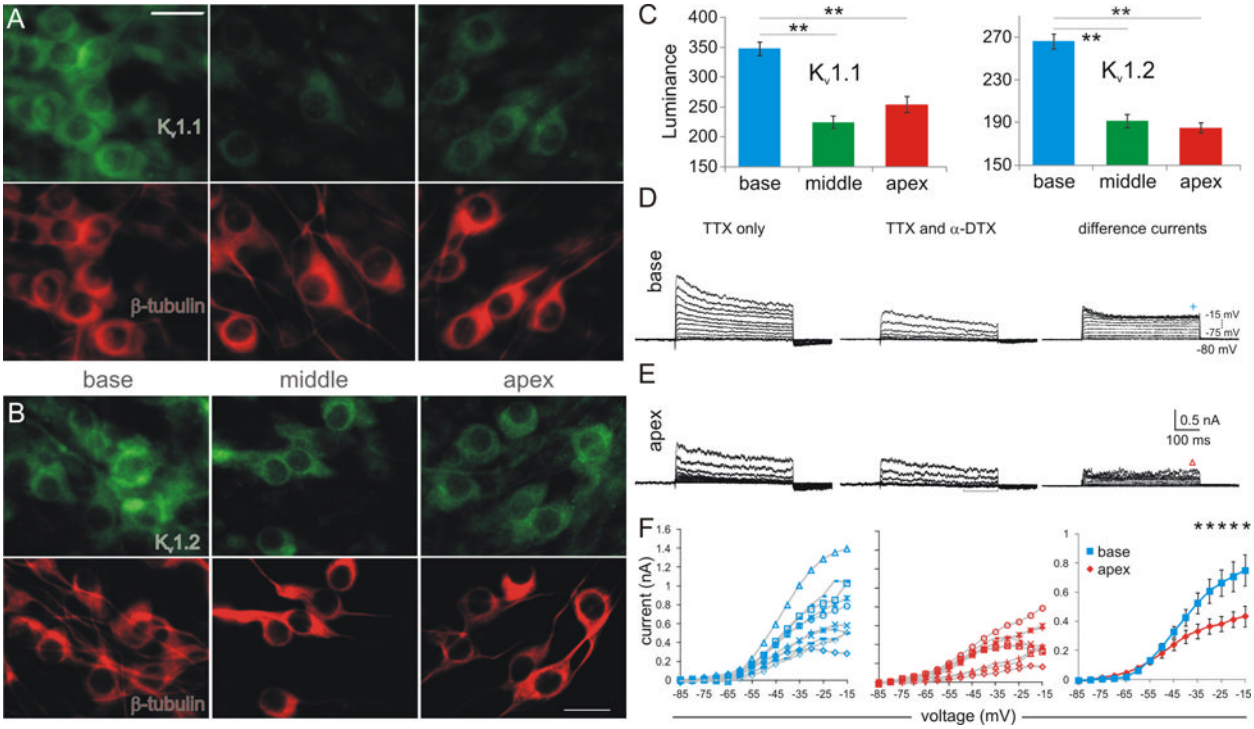

Fig. 3.

Anti-$K_v1.1$ and anti-$K_v1.2$ antibody somatic distribution along with DTX-sensitive K_v1 current magnitudes were greater in the base relative to middle and apex regions. (A-B) Immunostaining of α-subunits for $K_v1.1$ (A) and $K_v1.2$ (B) distribution (upper panels, green) in β-III-tubulin positive (lower panels, red) spiral ganglion neurons in the three regions of interest. Scale bar: 20 μm. (C) Average luminance from four separate experiments show enhanced $K_v1.1$ and $K_v1.2$ protein levels in the basal relative to the middle and apical neurons. Luminance from base to apex: $K_v1.1$, 348 ± 11, 224 ± 10, 254 ± 13; $K_v1.2$, 266 ± 7, 192 ± 6, 185 ± 5. (D-E) Whole-cell voltage clamp recordings of outward currents activated in response to 5mV voltage steps up to -15 mV from a holding potential of -80 mV before and after bath perfusion of α-DTX (left and middle panels with leak-subtraction) from a basal (D) and apical neuron (E). The difference currents (right panels) reflect the α-DTX sensitive component of K_v1 currents. These sweeps were created from non-leak subtracted traces in control and α-DTX conditions (see Methods). The bracket in E indicates possible I_h involvement in the leak-subtraction process. The symbol shape indicates which individual experiment is represented (from F); symbol location defines where the currents were measured for the current-to-voltage relationship as shown in F. (F) K_v1 current magnitudes plotted as a function of voltage levels for individual recordings (left panel, blue for base; middle panel, red for apex) and the average of all recordings in each group (right panel). The current magnitudes were significantly different at and above -35 mV, indicated by asterisks.

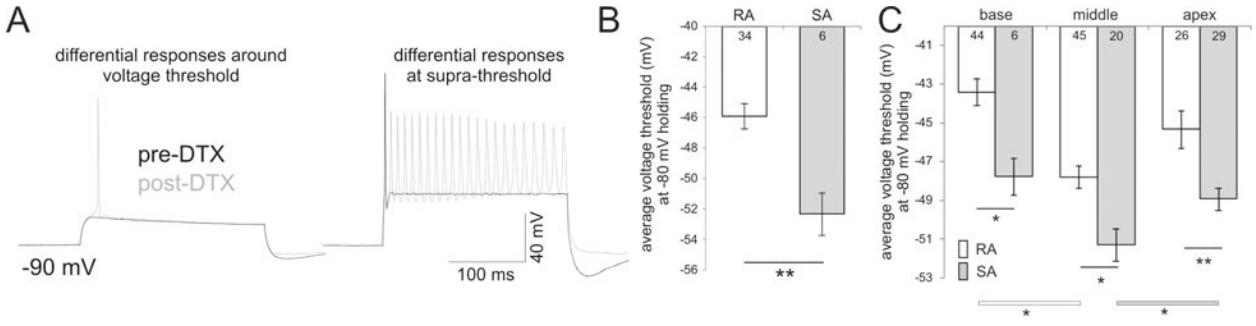

Fig. 4.

Rapidly accommodating (RA) neurons have significantly higher thresholds than slowly accommodating neurons (SA). (A) Transformation of rapidly accommodating neurons by α-DTX into slowly accommodating neurons occurs in conjunction with significantly altered threshold levels by α-DTX. Left set of traces show that at similar plateau voltages the same neuron that was originally below threshold prior to α-DTX application fired above threshold afterwards. Right set of traces demonstrate the accommodation differences before and after α-DTX application at supra-threshold levels. See text in Results section for RA versus SA distinction. (B) Average threshold comparison between RA and SA neurons demonstrating that RA neurons have higher average thresholds than SA neurons from a subset of recordings shown in Fig 1C. (C) Consistent and significant differences in voltage thresholds from base to apex are preserved in each category when RA and SA neurons are further separated by tonotopic region. Significant differences were observed between RA and SA neurons for each region ($p < 0.01$), between base and middle for RA neurons ($p < 0.05$) and between middle and apex for SA neurons ($p < 0.05$). The differences in the number of recordings between panels B and C reflect the inclusion of previously unpublished analysis (Liu and Davis, 2007) to power these comparisons. Note that the middle RA neurons displayed slightly reduced thresholds from their apical counterparts, yet differed significantly from the basal neurons (white bar with asterisk). When threshold level is evaluated for SA neurons, however, the values for middle neurons are significantly lower than apical (gray bar with asterisk) and slightly lower than basal neurons. The lack of significant difference between middle and base SA neurons is expected as only a small portion of SA neurons (N = 6) can be identified in the base.

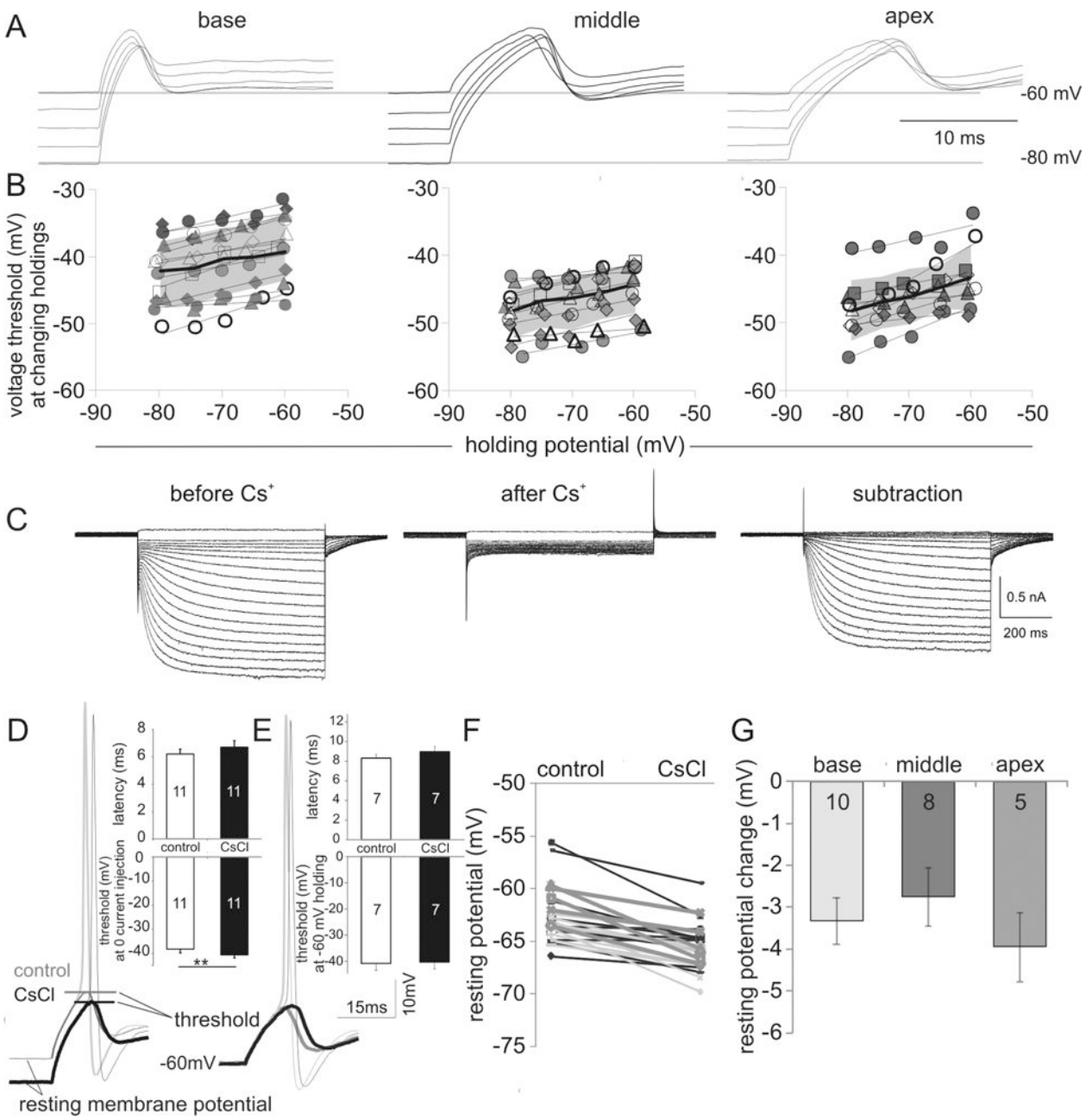

Fig. 5.

Blockade of I_h current with 5 mM CsCl hyperpolarizes neuronal resting potentials which, in turn, caused a predictable shift in threshold. (A) Altering holding potential causes concomitant changes in threshold. Traces show neuronal thresholds at five different holding potentials from -80 to -60 mV in 5 mV increments from individual basal, middle and apical neurons. (B) Threshold plotted against holding potential for each individual recording (symbols in different shapes or outlines) for base, middle and apex regions and for the group data (line and shadow plot). The thin black lines connect mean thresholds at each holding potential. Thick lines showed the means for each recording group with the gray background indicating one standard deviation. (C) Voltage clamp recording of inward currents in control (left) and CsCl conditions (middle); difference currents are shown on the right. Test potentials were from -55 mV to -160 mV in 5 mV intervals from a holding potential of -60

mV. The -60 mV trace at the same holding was not displayed. The specificity of Cs^+ on I_h was confirmed from the difference currents that show no observable outward component. (D) Sample apical neuron traces show a hyperpolarizing shift of resting potential subsequent to CsCl perfusion. The threshold changes accompanying the resting potential shift are expected from *A*. Insets show bar chart comparison of average latency (6.22 ± 0.34 ms vs. 6.71 ± 0.45 ms, n = 11) and threshold (-38.28 ± 1.46 mV vs. -40.66 ± 1.18 mV, n = 11, $p < 0.05$) before and after CsCl treatment with zero current injection. (E) Sample traces from a middle ganglion current clamp recording show no threshold changes after the holding potential was restored to -60 mV following perfusion of 5 mM CsCl. The action potential latency was prolonged in this cell from 7.3 to 9.2 ms by CsCl. Insets show bar chart comparison of average latency (8.32 ± 0.36 ms vs. 8.97 ± 0.52 ms, n = 7) and threshold (-40.8 ± 2.44 mV vs. -40.25 ± 2.49 mV, n = 7) before and after CsCl treatment. (F) Pair-wise comparison of resting membrane potential before and after CsCl treatment. (G) Bar chart comparison of the average resting potential change from base to apex.

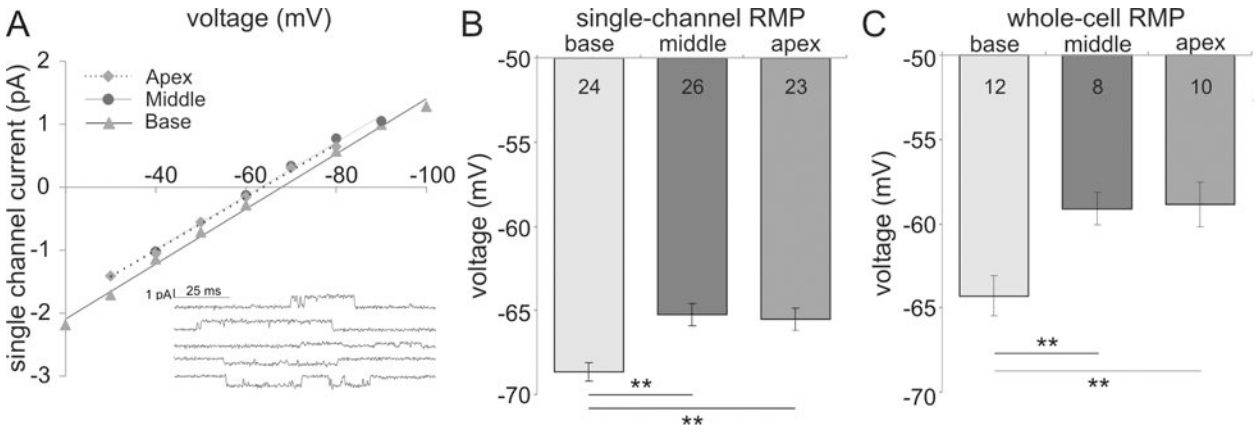

Fig. 6.

Endogenous resting membrane potentials show a nonlinear distribution along the cochlea that mirror the threshold distribution. (A) Single channel current-to-voltage relationships from individual base (filled triangle), middle (filled circle) and apex (filled diamond) neurons represent the differences in resting membrane potentials from base to apex. Inset shows examples of single channel currents at five test potentials (-100, -90, -70, -50, -40 mV). At reversal, the resting membrane potential is equal to the pipette potential therefore; the resting potential is more hyperpolarized in the base relative to the mid-apex. (B) The average resting membrane potentials from cell-attached single channel recordings show base neurons are the most hyperpolarized and middle neurons are slightly depolarized compared to the apex. (C) Measurement of resting potentials following membrane rupture for whole-cell current clamp mode showed values shifted to slightly more depolarized levels, yet showed a similar nonlinear trend as in *B*.

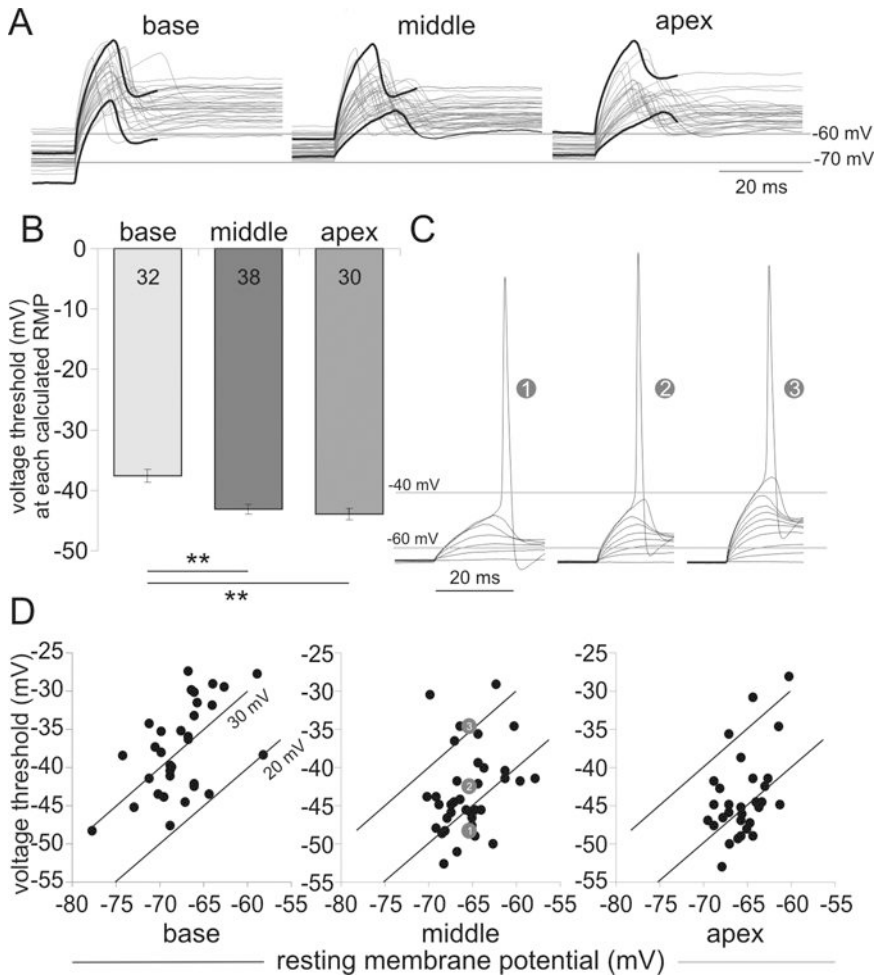

Fig. 7.

Differential voltage magnitude measured from endogenous resting potential to threshold demonstrates a nonlinear and heterogeneous distribution. (A) Overlay of threshold traces from multiple current clamp recordings, each held at its endogenous resting potential from the three cochlear regions. Black traces highlight the upper and lower extremes in threshold. (B) Average threshold (in mV, -37.59 ± 1.05, n = 32; -43.09 ± 0.9, n = 38; -43.91 ± 1.02, n = 30) from base to apex. (C) Three middle recordings (numbered symbols) with similar resting potentials show different threshold levels. Sub-threshold responses to increasing step current injection were overlaid for each recording. (D) Threshold plotted against resting potential for all recordings acquired in each region. Two differential voltage magnitudes of 20 and 30 mV are shown as a reference. Numbered gray circles indicate the three recordings shown in C.

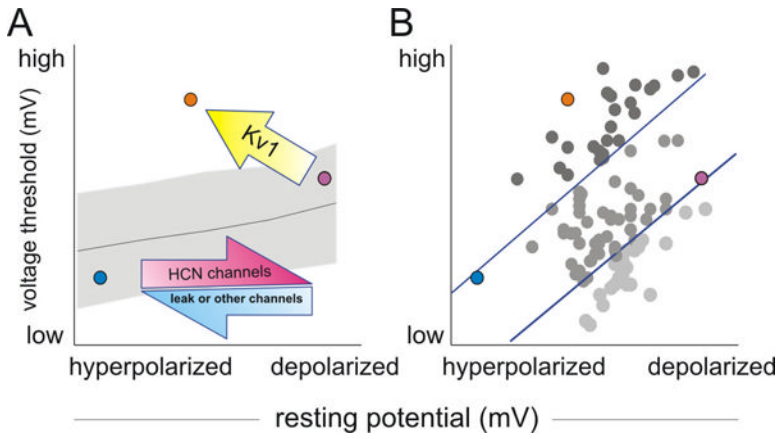

Fig. 8.

Depiction of the three currently identified mechanisms that primarily contribute to the diverse resting potential and threshold levels in cultured spiral ganglion neurons. (A) The blue and magenta arrows indicate the first mechanism of resting potential regulation. More HCN channels and potentially fewer leak channels or chloride channels or elevated Na^+/K^+-ATPase activity (Kim et al., 2007) would depolarize the resting potential along the x-axis. The line and shadow plot illustrate a second mechanism of indirect threshold regulation by resting potential. The combination of these two mechanisms slides the blue circle to the magenta position or vice versa. The third mechanism involves K_v1 regulation of threshold and resting potential. The yellow arrow indicates increasing K_v1 conductance could change the magenta circle to the orange position by elevating threshold and hyperpolarizing the resting potential. (B) The distribution of all neurons according to their threshold and resting potential could be explained by the three mechanisms outlined in A. The neurons were color coded based on their differential voltage magnitude above or below two arbitrary reference levels (blue lines).